Inorganic Chemistry

Communication

pubs.acs.org/IC

Lithium Cycling in a Self-Assembled Copper Chloride–Polyether Hybrid Electrode

Adam Jaffe and Hemamala I. Karunadasa*

Department of Chemistry, Stanford University, Stanford, California 94305, United States

Supporting Information

ABSTRACT: Atomic-scale integration of polyether molecules and copper(II) chloride layers in a two-dimensional perovskite affords, to the best of our knowledge, the first example of extended Li^+ cycling in a metal chloride electrode. The hybrid can cycle over 200 times as a cathode in a lithium battery with an open-circuit voltage of 3.2 V. In contrast, $CuCl_2$ alone or the precursors to the hybrid cannot be cycled in a lithium battery, demonstrating the importance of the layered, organic–inorganic architecture. This work shows that appropriate organic groups can enable Li^+ cycling in inexpensive, nontoxic, metal halide electrodes, which is promising for large-scale applications.

Metal oxides dominate the field of lithium battery cathode materials.[1] The stability of the O 2p band allows access to high metal oxidation potentials without material degradation, affording high cell voltages.[2] However, these oxides are conventionally synthesized at elevated temperatures (800–900 °C),[1,2] and high manufacture and precursor costs impede their use in large-scale, stationary applications.[3] Because of the similar electronegativity of oxygen and chlorine, metal chlorides are also candidates for high-voltage battery cathodes and may provide a route to reduce material synthesis temperatures. Several metal halide cathodes have been previously investigated for conversion reactions with lithium, including AgCl and $CuCl_2$. These electrodes showed poor cycling performance, attributed to material dissolution through the formation of soluble, reduced species.[4] To the best of our knowledge, Li^+ cycling has not been accomplished in metal chlorides. Here, we show that a hybrid structure featuring electrolyte-like organic groups in proximity to $Cu^{II}Cl$ layers can stabilize extended Li^+ cycling in an extremely low-cost and nontoxic material. Importantly, we show that $CuCl_2$ alone or a stoichiometric mixture of the precursors to the hybrid cannot be cycled in a lithium battery, demonstrating the importance of close integration between organic and inorganic components.

Two-dimensional hybrid perovskites[5] form layered metal halide structures similar in topology to Li^+-insertion compounds such as TiS_2 and $LiCoO_2$.[6] They are synthesized in solution under ambient conditions and can be isolated as polycrystalline powders or as oriented films. We used this platform to incorporate polyether molecules between $Cu^{II}Cl$ sheets. The ether groups were selected to mimic the coordination environment of Li^+ in ethereal solvents. High Li^+ mobility has been achieved in polyether-based solid electrolytes,[7] and we envisioned that placing polyether groups in proximity to the Cu^{2+} centers could lower the energetic cost of desolvation upon Li^+ intercalation and deter the formation of lithiated, soluble copper species.

Combining acidic ethanol solutions of $CuCl_2$ and $(EDBE)Cl_2$ [EDBE = 2,2′-(ethylenedioxy)bis(ethylammonium)] afforded $(EDBE)[CuCl_4]$ (**1**) as a crystalline solid. We obtained crystals suitable for structure solution by layering $(EDBE)Cl_2$ in 12 M HCl and $CuCl_2$ in a methanol–acetonitrile mixture. The crystal structure shows sheets of corner-sharing Cu–Cl octahedra with bridging equatorial chlorides (Figure 1). A pronounced Jahn–

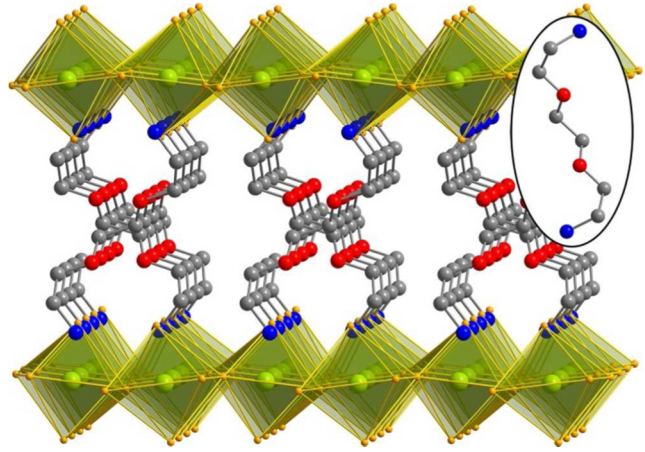

Figure 1. X-ray structure of **1**. Inset: an EDBE dication. H atoms omitted for clarity. Green, orange, red, blue, and gray spheres represent Cu, Cl, O, N, and C atoms, respectively.

Teller distortion of the d^9 Cu center is evident with Cu–Cl distances of 3.1009(6) and 2.3059(6) Å. Similar to other $Cu^{II}Cl$ perovskites,[8] the elongated Cl–Cu–Cl axis orders in an antiferrodistortive arrangement in the plane of the inorganic sheets (Figure S4 in the Supporting Information, SI). Hybrid perovskites typically form dense structures. Fortuitously, the crystal structure of **1** shows adjacent polyether chains crossing to create ca. 0.7-Å-diameter channels that traverse the material.

To test if Li^+ can be cycled through **1**, we obtained solid-state cyclic voltammograms (CVs) in a flooded three-electrode cell with Li^0 counter and reference electrodes (Figure 2a). The CV obtained in a tetrabutylammonium (Bu_4N^+) hexafluorophosphate electrolyte shows no significant redox processes. The same

Received: April 14, 2014
Published: June 11, 2014

   dx.doi.org/10.1021/ic500860t | *Inorg. Chem.* 2014, 53, 6494–6496

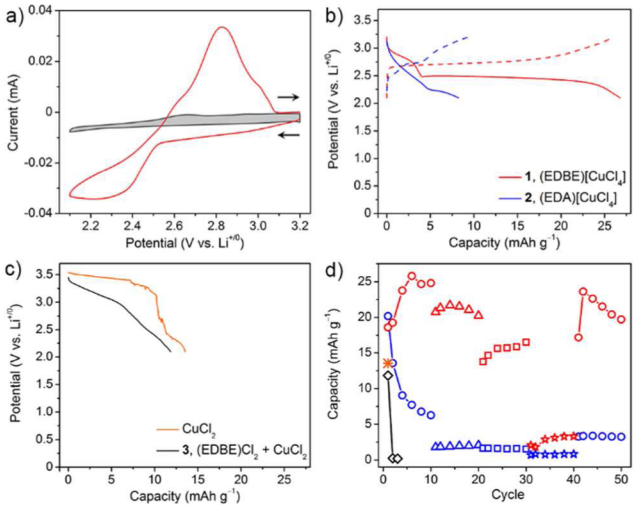

Figure 2. Electrochemistry of **1**, **2**, **3**, and $CuCl_2$ at 22 °C: (a) CVs of **1** on a carbon electrode in Li^+ (red) and Bu_4N^+ (gray) electrolytes. The current attributed to double-layer capacitance is shaded in gray (10 mV·s^{-1}; Li^0 counter and reference electrodes). (b) Typical discharge (solid line) and charge (dashed line) profiles at 28 mA·g^{-1} for **1** (red) and **2** (blue). (c) Irreversible discharge curves for $CuCl_2$ (orange) and **3** (black). (d) Cycling capacity for **1** (red) and **2** (blue) at 28 (circles), 57 (triangles), 114 (squares), and 341 (stars) mA·g^{-1}. Capacities (28 mA·g^{-1}) for the irreversible discharge of $CuCl_2$ (orange) and **3** (black). Capacities are normalized to their molar equivalent of **1**.

electrode was then immersed in a lithium bis(trifluoromethane)-sulfonimide electrolyte, and the CV was recorded again. It shows distinct waves consistent with Cu^{2+} reduction accompanied by Li^+ introduction into the material. The bulkier Bu_4N^+ cation is less likely to insert and should only be involved in surface interactions, allowing us to decouple the current arising from double-layer capacitance from the overall current (Figure 2a).[9] A broad reduction wave in the Li^+ electrolyte occurs with an onset of 3.01 V that gradually increases in current until a more defined reduction wave appears that peaks at 2.24 V vs $Li^{+/0}$. The return scan shows a depressed current profile at low potentials until a broad oxidation wave occurs with a peak at 2.83 V vs $Li^{+/0}$ that is coupled to both reduction events. The depressed current in the oxidative scan is likely due to incomplete reaction of the active material in the reductive scan. (The reductive scan was reversed at 2.1 V vs Li^+ to avoid a second irreversible reduction described later.) Current integration (Figure S5 in the SI) and galvanostatic cycling experiments (Figure 2b) show charge conservation between the redox processes.

Encouraged by these results, we tested **1** in coin cells with Li^0 counter electrodes. Cells were galvanostatically cycled between discharge and charge potential limits of 2.1 and 3.2 V vs $Li^{+/0}$, respectively. The open-circuit voltage of 3.2 V compares favorably with systems considered for grid-scale applications, such as lead–acid (2.1 V), nickel–cadmium (1.35 V), and $Li_4Ti_5O_{12}$–$LiFePO_4$ (1.7 V).[3] The discharge curve (Figure 2b) shows two steps corresponding to the two reduction events evident in the CV. The symmetry of the charge and discharge profiles and small separation between voltage plateaus indicate efficient Li^+ cycling. Without electrode optimization, we obtain average Coulombic efficiencies of 92(4)% and round-trip energy efficiencies of 96(3)% at a current density of 28 mA·g^{-1}. The reductions occur at values more negative than the calculated voltage for the first reduction in a Li–$CuCl_2$ cell: Cu^{2+}/Cu^+ at 3.62 V vs $Li^{+/0}$.[10] The shift in potential for the redox events in **1** could be due to the anionic inorganic sheets or kinetic limitation of Li^+ transport. X-ray photoelectron spectroscopy measurements on discharged electrodes confirm a one-electron reduction to form Cu^{1+} (Figure S9 in the SI), and impedance spectroscopy shows ionic conductivity for discharged (lithiated) electrodes (Figure S10 in the SI).

Electrodes containing **1** could cycle over 200 times at a rate of 28 mA·g^{-1} (22 μA·cm^{-2}; Figure 3). The theoretical specific

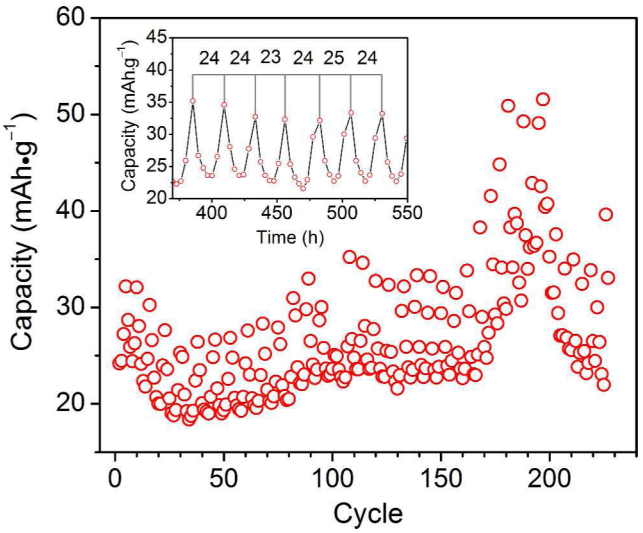

Figure 3. Capacity versus cycle number for a **1** cell cycled between 2.1 and 3.2 V vs $Li^{+/0}$ at 28 mA·g^{-1} (*C*/3). Inset: Capacity changes as the cell heats (from 22–40 °C) over 24-h periods.

capacity of **1** for a one-electron reduction is 75 mAh·g^{-1}, and extended cycling affords capacities of up to 52 mAh·g^{-1}. Because temperature fluctuations are common in large-scale battery installations, we allowed the cell to heat by the sun over 24-h periods and measured average gravimetric capacities (according to the active mass) over 225 cycles of 38(6) mAh·g^{-1} at 40 °C and 26(4) mAh·g^{-1} at 22 °C. Increases in capacity during later cycles may be due to morphological changes in the material that modify electrical contact with the current collectors. Most inorganic electrodes undergo significant structural and volumetric changes upon (de)lithiation. Along with internal cell resistance, this results in heat generation during Li^+ cycling. The pliable organic groups in **1** should reduce volume changes upon Li^+ cycling compared to inorganic electrodes, and sustained performance throughout temperature ranges encountered in large battery stacks (40–60 °C) is an advantage.[11] Importantly, the cell capacity did not gradually decrease with time. Instead, the cell failed abruptly at the 227th cycle when the voltage dropped to 0 V. This indicates device failure through a short circuit and not material degradation and may be circumvented through device optimization. While the capacity of **1** must improve for applications, this demonstrates that hybrids with appropriate organic functionalities enable Li^+ cycling in metal halide electrodes. Such inexpensive, nontoxic electrodes are especially attractive for grid-scale energy storage. Here, cells can be placed in parallel to achieve higher combined capacities, and cost, safety, and lifetime take precedence over gravimetric capacity.[3]

To assess the importance of the hybrid structure for Li^+ cycling, we studied three controls: (i) solid $CuCl_2$; (ii) a hybrid perovskite containing alkyl instead of polyether groups, (EDA)-$[CuCl_4]$[8] (**2**, where EDA = ethylene-1,2-diammonium); (iii) a

dx.doi.org/10.1021/ic500860t | *Inorg. Chem.* 2014, 53, 6494–6496

stoichiometric mixture (**3**) of the precursors to **1**: $(EDBE)Cl_2$ and $CuCl_2$. Their reported capacities (Figure 2b–d) are normalized to the molar equivalent of **1**. The $CuCl_2$ control shows an initial capacity of 13.5 $mAh{\cdot}g^{-1}$, but it cannot be cycled further. When we attempt to charge $CuCl_2$ cells, the voltage drops close to 0 V vs $Li^{+/0}$ (Figure S11 in the SI). Disassembled cells reveal that $CuCl_2$ has dissolved and plated on the Li^0 electrode. The charge/discharge profiles for **2** begin with a capacity of 20 $mAh{\cdot}g^{-1}$ that falls during the first 10 cycles to a low cycling capacity of 4–5 $mAh{\cdot}g^{-1}$, indicating the importance of the polyether groups for Li^+ cycling. An electrode with **3** was assembled under rigorously anhydrous conditions to prevent the formation of **1** [as verified by powder X-ray diffraction (PXRD) before and after cycling; Figure S12A in the SI]. This cell could not be cycled (Figure 2), demonstrating the importance of the close integration of organic–inorganic components in **1**.

Interestingly, **1** also serves as a precursor to a negative electrode, albeit with low capacity. When a cell containing **1** is cycled between 2.5 and 0.3 V vs $Li^{+/0}$, the first discharge profile shows an irreversible reduction at 1.9 V vs $Li^{+/0}$ (Figure S13 in the SI). The reduced material can then be cycled at a rate of 28 $mA{\cdot}g^{-1}$ (22 $\mu A{\cdot}cm^{-2}$) with high reversibility, an average Coulombic efficiency of 99(2)%, and a round-trip energy efficiency of 66(1)% over 700 cycles with a stable capacity of 14(1) $mAh{\cdot}g^{-1}$. The contribution from Li^+ insertion into the carbon additive (which must be considered for anodic cycling) has been subtracted from this value (Figure S15 in the SI). This cell also abruptly failed after the 716th cycle, likely because of device failure. Cells containing $CuCl_2$ fail after just two cycles, and cells containing **2** show no additional capacity above that of the carbon additive (Figure S16 in the SI).

We obtained PXRD data of electrodes from disassembled cells at various states of (dis)charge. Several reflections from **1**, including the (200) reflection at 7.4° that corresponds to lattice planes parallel to the inorganic layers, are retained in electrodes cycled from 3.2 to 2.1 V vs $Li^{+/0}$ (Figure S17 in the SI). The (200) reflection evolves into a broad hump in an electrode that was cycled 100 times, possibly because of material exfoliation or a range of low-angle reflections from different lithiation states. New reflections are also evident in electrodes discharged to 2.1 V and then charged back to 3.2 V vs $Li^{+/0}$. The reproducible voltage plateaus and low-angle PXRD peaks maintained even after 100 cycles in the cathodic range corroborate Li^+ cycling in an ordered material. Electrodes cycled anodically, past the irreversible voltage plateau at 1.9 V, no longer show the (200) reflection (Figure S18 in the SI). A weak reflection at 43.3° can be indexed to the PXRD pattern of copper metal.

We show Li^+ cycling with high Coulombic and energy efficiencies in a CuCl–polyether hybrid synthesized at room temperature. This is, to the best of our knowledge, the first demonstration of extended Li^+ cycling in a metal chloride cathode. The electrochemical behavior of **1** is consistent with a conversion reaction[12] stabilized by the integration of organic and inorganic components, an intercalation mechanism aided by the affinity of polyether groups for Li^+, or a combination of the two. Control experiments show the importance of the preassembled, layered architecture of **1** for Li^+ cycling. These hybrids can allow for organic and inorganic components to be optimized independently. Accordingly, we will attempt to increase the energy density of hybrid electrodes through inorganic substitution and tune the organic groups to improve Li^+ diffusivity.

■ ASSOCIATED CONTENT

Supporting Information

Crystallographic information, spectra, and experimental details. This material is available free of charge via the Internet at http://pubs.acs.org. The CIF for $(EDBE)[CuCl_4]$ has also been deposited in the Cambridge Crystallographic Data Centre under deposition number CCDC 973904. The file can be obtained, upon request, from the Director, Cambridge Crystallographic Data Centre, 12 Union Road, Cambridge CB2 1EZ, U.K.

■ AUTHOR INFORMATION

Corresponding Author

*E-mail: hemamala@stanford.edu.

Notes

The authors declare no competing financial interest.

■ ACKNOWLEDGMENTS

This work was funded by the National Science Foundation CAREER award (Grant DMR-1351538). A.J. is grateful for the Satre Family Stanford Interdisciplinary Graduate Fellowship. Single-crystal and powder X-ray diffraction studies were performed at the Stanford Nanocharacterization Laboratory. We thank Wesley Zheng and Prof. Yi Cui for helpful discussions and technical assistance.

■ REFERENCES

(1) (a) Whittingham, M. S. *Chem. Rev.* **2004**, *104*, 4271–4302. (b) Ellis, B. L.; Lee, K. T.; Nazar, L. F. *Chem. Mater.* **2010**, *22*, 691–714.
(2) Goodenough, J. B.; Kim, Y. *Chem. Mater.* **2009**, *22*, 587–603.
(3) Yang, Z.; Zhang, J.; Kintner-Meyer, M. C. W.; Lu, X.; Choi, D.; Lemmon, J. P.; Liu, J. *Chem. Rev.* **2011**, *111*, 3577–3613.
(4) (a) Salomon, M. *Pure Appl. Chem.* **1998**, *70*, 1905–1912. (b) Eichinger, G.; Besenhard, J. O. *J. Electroanal. Chem. Interfacial Electrochem.* **1976**, *72*, 1–31.
(5) (a) Mitzi, D. B. *Progress in Inorganic Chemistry*; Wiley-VCH: Weinheim, Germany, 1999; pp 1–121. (b) Mitzi, D. B. *J. Chem. Soc., Dalton Trans.* **2001**, 1–12.
(6) Winter, M.; Besenhard, J. O.; Spahr, M. E.; Novák, P. *Adv. Mater.* **1998**, *10*, 725–763.
(7) (a) Dupon, R.; Whitmore, D. H.; Shriver, D. F. *J. Electrochem. Soc.* **1981**, *128*, 715–717. (b) Armand, M. B.; Bruce, P. G.; Forsyth, M.; Scrosati, B.; Wieczorek, W. *Energy Materials*; John Wiley & Sons, Ltd.: New York, 2011; pp 1–31. (c) Croce, F.; Appetecchi, G. B.; Persi, L.; Scrosati, B. *Nature* **1998**, *394*, 456–458.
(8) Tichy, K.; Benes, J.; Halg, W.; Arend, H. *Acta Crystallogr., Sect. B* **1978**, *34*, 2970–2981.
(9) Brezesinski, T.; Wang, J.; Tolbert, S. H.; Dunn, B. *Nat. Mater.* **2010**, *9*, 146–151.
(10) Huggins, R. A. *Advanced Batteries: Materials Science Aspects*; Springer: New York, 2009.
(11) Spotnitz, R. In *Advances in Lithium-Ion Batteries*; Schalkwijk, W., Scrosati, B., Eds.; Springer: New York, 2002; pp 433–457.
(12) Cabana, J.; Monconduit, L.; Larcher, D.; Palacín, M. R. *Adv. Mater.* **2010**, *22*, E170–E192.